View metadata, citation and similar papers at core.ac.uk

brought to you by CORE

provided by Online Research Database In Technology

Technical University of Denmark

Fabrication of Nanostructures by Roll-to-Roll Extrusion Coating

Murthy, Swathi; Matschuk, Maria; Huang, Qian; Mandsberg, N.K.; Feidenhans'l, Nikolaj Agentoft; Johansen, P.; Christensen, L.; Pranov, H.; Kofod, G.; Pedersen, Henrik Chresten; Hassager, Ole; Taboryski, Rafael J.

Published in:
Advanced Engineering Materials

Link to article, DOI:
10.1002/adem.201500347

Publication date:
2015

Document Version
Peer reviewed version

Link back to DTU Orbit

Citation (APA):
Murthy, S., Matschuk, M., Huang, Q., Mandsberg, N. K., Feidenhans'l, N. A., Johansen, P., ... Taboryski, R. J. (2015). Fabrication of Nanostructures by Roll-to-Roll Extrusion Coating. Advanced Engineering Materials, 18(4), 484-489. DOI: 10.1002/adem.201500347

DTU Library
Technical Information Center of Denmark

General rights
Copyright and moral rights for the publications made accessible in the public portal are retained by the authors and/or other copyright owners and it is a condition of accessing publications that users recognise and abide by the legal requirements associated with these rights.

- Users may download and print one copy of any publication from the public portal for the purpose of private study or research.
- You may not further distribute the material or use it for any profit-making activity or commercial gain
- You may freely distribute the URL identifying the publication in the public portal

If you believe that this document breaches copyright please contact us providing details, and we will remove access to the work immediately and investigate your claim.

DOI: 10.1002/((please add manuscript number))
Article type: Communication

Fabrication of nanostructures by roll-to-roll extrusion coating

*Swathi Murthy, Maria Matschuk, Qian Huang, Nikolaj K. Mandsberg, Nikolaj A. Feidenhans'l, Peter Johansen, Lars Christensen, Henrik Pranov, Guggi Kofod, Henrik C. Pedersen, Ole Hassager, Rafael Taboryski**

Ms. S. Murthy, Dr. M. Matschuk, Dr. H. Pranov, Dr. G. Kofod
Inmold A/S, Diplomvej 381, DK-2800 Kongens Lyngby, Denmark

Ms. S. Murthy, Prof. Henrik C. Pedersen
Department of Photonics Engineering, Technical University of Denmark, Frederiksborgvej 399, DK-4000 Roskilde, Denmark

Dr. Q. Huang, Prof. O. Hassager
Department of Chemical and Biochemical Engineering, Technical University of Denmark, Søltofts Plads, building 229, DK-2800 Kongens Lyngby, Denmark

Mr. N. A. Feidenhans'l
Danish Fundamental Metrology A/S, Matematiktorvet 307, Kgs. Lyngby, Denmark

Mr. N. Mandsberg, Mr. Nikolaj A. Feidenhans'l, Prof. R.Taboryski
Department of Micro- and Nanotechnology, Technical University of Denmark, Ørsteds Plads, building 345b, DK-2800, Kongens Lyngby, Denmark
E-mail: rata@nanotech.dtu.dk

Mr. Peter Johansen, Mr. Lars Christensen, Danapak Flexibles A/S, Strudsbergsvej 3, DK-4200 Slagelse, Denmark

The drivers in the development of large area micro- and nanostructuring roll-to-roll (R2R) methods have been hologram security stickers, flexible electronics, graphene electrodes, and organic solar cells.[1] In terms of productivity for large area nanostructuring, the most established technology is roll-to-roll UV assisted nanoimprint lithography (R2R-UV-NIL), as demonstrated by Ahn et al, who reported replication of 300 nm line gratings using UV-curable imprint resist at a line-speed of 1 m/min.[2, 3] This method is limited in the choice of materials by the requirement of photo-curability. The throughput for current R2R-UV-NIL systems amounts to ~0.2 m^2/s. Another widely used technology is R2R hot embossing (R2R-

HE), in which a heated structured roller is used to emboss a structure into a thin film in a R2R process.[4, 5] The full potential of extending R2R techniques to nanostructuring of biomimetic functionalities such as super-hydrophobic[6], anti-reflective [7], structural and plasmonic color effects[8], is however today impeded by the relatively low throughput of R2R-UV-NIL and R2R-HE.[4, 9] These limitations seem associated with the rheology of polymer flow and the rate of UV-curing processes.[3]

This paper investigates a novel R2R process for nano- and microstructuring, potentially having improved productivity with rates exceeding 5 m^2/s (**Figure 1**). The process is known as roll-to-roll extrusion coating (R2R-EC, in the packaging industry commonly referred to as co-extrusion), which is widely used for production of smooth polymer films. Among benefits of R2R-EC are availability of a wide range of commercial extruders, off-the-shelf extrusion grade polymers, functional additives, polymeric materials with good diffusion barrier properties, and the overall maturity of the technology. However, only few studies have been devoted to this process. Frenkel et al.[10] reported replication by R2R-EC of sawtooth microstructures with line-speed 10 m/min, while Sollogoub et al.[11] described the rheological processes associated with standard R2R-EC. To our knowledge, there is no work describing production of nanostructured polymer films by R2R-EC so far.

In R2R-EC a molten polymer film (melt curtain) is extruded through a flat nozzle, then stretched in air, and finally laminated onto a carrier foil (substrate). The lamination process takes place as the melt curtain is squeezed between a structured cooling roller and a rubber counter roller. A force is exerted on the compliant counter roller to form a so-called nip region where the molten polymer solidifies and adheres to the carrier foil as shown in Figure 1a. Compared to R2R-UV-NIL and R2R-HE, the extrusion coating process is much faster, mainly due to the fact that the polymer is molten to begin with, and cools rapidly by contact with the cooling roller. When compared to other R2R techniques, R2R-EC resembles R2R-HE, in respect to pressure ranges, but is much less affected by the slow creep-strain effects

encounered in R2R-HE.[4] R2R-EC can also be compared to the polymer injection molding (IM) process.[12] In IM, the polymer is also molten at the onset of relief filling. Important differences between R2R-EC and IM are however the pressure and rheological conditions during relief filling. The nip pressure in R2R-EC is low (~20 bar), while injection pressures for IM typically reach much higher values (~1000 bar). In addition, for IM, the shear stress typically exceeds the critical value for wall slip, [13] whereas this is not the case in R2R-EC, where the shear rate in the nip is practically zero.[11] Most extruders have multi-feed nozzles, allowing for e.g. an adhesion layer to be co-extruded with the structure layer for better adhesion to the carrier foil. If a relief structure is attached to the surface of the cooling roller, the pressure buildup in the nip will force intrusion of the molten polymer into the relief structure, which is the topic of investigation in this paper. R2R-EC is simpler than R2R-UV-NIL, as it does not require any curing step.

We demonstrate large area replication at high throughput of patterns both on micrometer- (Figure 1b, c) and nanometer scale (**Figure 2**) in thermoplastic foils using standard industrial R2R-EC equipment and standard thermoplastic polymers. We argue that different regimes of replication exist; a nanostructure regime, where replication is dominated by surface tension of the melt in the nip, and a microstructure regime where microscopic flow is required to fill the deeper microstructures. Nanostructures with typical linewidth in the range 100 - 400 nm are best replicated using semi-crystalline polymers such as polypropylene (PP), running at high roller line-speed V_R, and high cooling roller temperature T_c (Figure 2). The best replication of nanopillars (diameter: 120 nm and height: 100 nm in Si master) was obtained for $T_C = 70°$ C and the highest line-speed $V_R = 60$ m/min (Figure 2a,b), whereas e.g. at $T_C = 30°$ C and $V_R = 10$ m/min, the pillars were only 50% replicated in terms of height compared to the Si master (Figure 2c,d,e). For the used parameter range, this degree of replication at nanoscale was only achieved in PP. Replication in other common polymers like polyethylene (PE) and

polystyrene (PS) was not possible for nanostructures.[14] Structures with linewidths and depths above ca. 400 nm seem to belong to a different replication regime allowing for a wider range of materials.[14] For microstructures (see Figure 1c), we find that process parameters (V_R, F, T_C) have to be individually optimized for each pattern, indicating that viscoelastic flow into the relief plays a more important role.[4] We believe this difference originates from the thermo-mechanical conditions in the nip as shown in **Figure 3**. Both nano- and microstructures require a pressure buildup in the nip for good replication. This is achieved by the compliance of the rubber counter roller. We adapted the theory for contact between two deformable solids to predict the pressure profile in the nip.[11, 15] A force F is applied to the counter roller resulting in a pressure within the nip,

$$P_{nip} = P_{max}\sqrt{1-\left(\frac{L_{nip}-2x}{L_{nip}}\right)^2}, \qquad (1)$$

where $P_{max} = F/(\pi W L_{nip})$, x is the distance along the nip from the entrance, L_{nip} is the length of the nip region (see Figure 1a), and W is the width of the rollers. The calculated pressure curves in the nip for three different force values are shown in Figure 3b. According to Equation 1, the maximum pressure is reached at the center of the nip. The carrier foil and the polymer passage in the nip do not significantly affect the pressure in the nip.

We modelled the temperature profile along the nip in a 100 µm thick polymer melt sandwiched between the Ni mold and the polyethylene terephthalate (PET) carrier foil.[14] The model simulates the temperature variation at different distances from the mold surface in the polymer along the nip. Our primary interest for this investigation is the cooling rate in the polymer melt near the mold-polymer interface. The model shows that the polymer melt cools very rapidly near the mold surface. In fact it cools even before entering the nip. The cooling rate is of the order of 10^7 K /s at a distance 100 nm from the mold once it enters the nip, while it cools much slower in the bulk of the polymer melt away from the mold surface (Figure 3c).

The high rate is due to the high thermal conductivity of Ni as compared to polymer. The line-speed is an important factor affecting the temperature profile in the nip (Figure 3). At higher line-speed the polymer solidifies further into the nip and the polymer melt experiences higher nip pressure before solidification of the surface region (Figure 3).

The low pressure and the absence of shear stress in the nip indicate that no-slip boundary conditions are expected to hold for nanopattern filling in the mold.[13, 16] For a pressure ΔP across the melt/air interface, the radius of curvature R is given by the Young-Laplace formula:

$$R = \frac{-2\gamma(T)\cos\theta_a}{\Delta P}, \qquad (2)$$

where $\gamma(T)$ is the temperature-dependent surface tension, while θ_a is the advancing contact angle for the polymer melt intruding into the mold relief. As the antistiction coating[14, 17] of the roller ensures $\theta_a \sim 120°$, and hence $\cos\theta_a \sim -1/2$, we argue that feature sizes smaller than $R \sim \gamma(T)/\Delta P$ cannot be replicated. The surface tension for polymer melts is known to decrease linearly with temperature: [16, 18]

$$\gamma(T) = \gamma_0 - \alpha T. \qquad (3)$$

For PP we used $\gamma_0 = 27.734$ mN/m and $\alpha = 0.059$ mN/(m °C) reported by Duo Yang et.al..[16] The crystallization temperature obtained by differential scanning calorimetry (DSC) in this work is ~120° C at a cooling rate of 10 K/min. However, PP is a semi-crystalline polymer, and we expect considerable crystallization retardation for the extremely high cooling rate (~10^7 K/s) near the mold.[19] The polymer melt is thus expected to be supercooled and solidify at much lower temperature $T \gtrsim T_C = 70°$ C. If we conservatively assume solidification at the temperature 120° C, we can follow the 60 m/min curve (100 nm from the mold surface) in Figure 3d to arrive at a distance of ~ 1 µm inside the nip for $T = 120°$ C. At this distance, the nip pressure is ~ 0.3 bar. The characteristic radius of curvature R for the PP melt under 0.3 bar and 120° C is ~ 650 nm calculated from Equation 2 and 3. In order to

completely fill the nanoholes in the mold, including the corners, R should be smaller than the radius of the nanoholes, i.e. $R \lesssim 60$ nm for 120 nm pillars (Figure 2). Since smaller pillars were actually replicated at these conditions, this clearly indicates that supercooling of the polymer melt must play an important role in the process. To confirm this hypothesis, we tried to replicate nanopatterns using other polymers, polystyrene (PS) and polyethylene (PE). For PS the glass transition temperature (T_g) is ~100° C, while the solidification temperature for PE is ~110° C. PS is an amorphous polymer; it solidifies below T_g and cannot be supercooled. Indeed, for the parameter range used in this investigation, it was not possible to achieve a visible replication of structures in PS. Though PE is a semi-crystalline polymer and can be supercooled, its crystallization rate is extremely high (compared to PP), which means that PE solidifies quickly below its static solidification temperature (110° C).[20] Hence, R does not become small enough to fill the nanoholes in the mold for PS and PE. From Figure 2, we see that the cooling rate of the PP melt near the mold is ~10^7 K/s at $V_R = 60$ m/min. We cannot measure the crystallization rate of PP at such high cooling rate as the maximum cooling rate that presently can be attained by flash DSC is ~10^4 K/s.[21] However, the half crystallization time for PP at 80° C is reported to vary from 0.2 to 10 seconds.[21, 22] The polymer takes about 9 ms to reach the center of the nip (9 mm at 60 m/min), where the pressure is maximum and hence R is minimum. Since we observe complete replication of nanopillars at 60 m/min, it indicates retardation of solidification of PP by a sufficient amount of time to attain a small enough R. This explains why the replication of nanopillars (Figure 2) diminishes at lower V_R and lower T_c. We observed incomplete replication of 40 nm structures and take this as the lower limit for replication in the model.

In conclusion, we have demonstrated replication of micro- and nanostructures in thermoplastic polymers, by a very high throughput, industrial process R2R-EC. Structures of different dimensions, shapes and aspect ratios have been replicated with high replication

fidelity, and productivity up to 0.45 m^2/s. Nanostructures down to 80 nm and height 100 nm could be replicated in PP at $V_R = 60$ m/min. The limiting factors for proper replication of nanostructures were found to be the surface tension induced radius of curvature of the polymer melt and the retardation time for crystallization of the melt. The retardation time limitation leads to the surprising feature of the process, that the replication quality of nanostructures in crystalline polymers becomes better the higher line-speed is used.

We suggest that the discovery of accurate and high productivity nano- and microscopic replication in thermoplastic materials could accelerate the integration of nanostructured materials in a broad range of applications, including optical, technical and functional surfaces and devices. Further possible applications may include cast molding of advanced materials for photo-voltaic, thermo-electric, electro-active and electro-storage applications, where nanostructuring often leads to improved properties.

Experimental section

The nano-microstructured foils were produced by extrusion coating on a pilot roll-to-roll extrusion coating machine, at Danapak Flexibles, Slagelse, Denmark. It consists of a 25 mm extruder (BfA Plastic GmbH), 35 mm extruder (AXON Plastics Machinery AB), and an EPOCH nozzle with a respective 3-layer feedblock (Cloeren Inc). Micro-nanostructured Ni molds where fabricated by a dry etching, electroplating and molding (DEEMO) process.[14, 23] The Ni molds were simply glued to the cooling roller (width $W = 45$ cm, diameter $D_{cool} = 27.2$ cm) with double sided adhesive tape. The cooling roller is cooled by water, and its temperature T_c was kept below the solidification temperature of the polymer. The counter roller (diameter $D_{counter} = 12.5$ cm) consisted of a metal core wrapped with a ~10 mm thick layer of silicone rubber, making it flexible on the surface. The counter roller was maintained at room temperature using cooling water. The force F applied across the nip was provided by

two hydraulic pistons, one attached at each end. The nip length L_{nip} was measured by running a deformable tape through the nip at different applied force F and measuring the length of the deformation in the tape. The force across the nip is exerted by two hydraulic pistons attached to the counter roller. F is calculated by multiplying the measured oil pressure P_{oil} in the pistons with the surface area of the pistons. The rollers are not motorized; their drive is supplied by the substrate drawn by the winder, creating a line tension, and resulting in a line-speed V_R. PP was co-extruded with a polyethylene (PE) adhesion layer material at 295° C and laminated onto a polyethylene terephthalate (PET) carrier foil.

The solidification temperature was measured by differential scanning calorimetry (DSC) (DSC-Q1000, TA Instruments)(Figure S7).[14]

We investigated the nano-microreplication ability of various polymers, like pure PP (WF420HMS, Borealis), low density polyethylene (LDPE - 3020D, LyondellBasell), polyethylene modified polypropylene (hereafter referred to as polyolefin, PO), polymethylpentene, polystyrene (PS: BASF PS 158K) and cyclic olefin copolymer (Topas 8007X4, Topas Advanced Polymers GmbH).[14] Different sets of processing parameters were investigated to assess their influence on the replication fidelity.[14] Specifically, the influence of cooling roller temperature T_c (30° C to 70° C), Line-speed V_R (10 m/min to 60 m/min) and nip force F (7 to 30 kN/m) were explored separately, while keeping all other parameters constant.[14] For the parametric analysis, extruder output, melt temperature, feed rate, die-gap, and air-gap height were kept constant. For each set of process parameters, several hundred meters of polymer foil were produced. The replication was assessed and compared for samples across different parameter sets. Several samples were cut from the same foils to assess the homogeneity of replication. The structures shown in this paper were characterized either by scanning electron microscopy (SEM - Zeiss Supra) or by atomic force microscopy

(AFM - Park Systems Corporation XE-150). Prior to SEM, the polymer foils were coated with a ~10 nm thin film of gold-palladium.

Supporting Information

Supporting Information is available from the Wiley Online Library or from the author.

Acknowledgements

This work is supported by the Danish National Advanced Technology Foundation (HTF) through the "Advanced Technology Project LANI" (grant 011-2011-3), the "Advanced Technology Platform NanoPlast" (grant 007-2010-2), and by The Danish Ministry of Higher Education and Science, through an industrial PhD scholarship for Swathi Murthy (grant 1355-00143). Mr. Nis K. Andersen, Mr. Freddy Lang, and Ms. Nanna Bild are acknowledged for help with the artwork.

Swathi Murthy and Maria Matschuk contributed equally to this work.

Received: ((will be filled in by the editorial staff))
Revised: ((will be filled in by the editorial staff))
Published online: ((will be filled in by the editorial staff))

References

[1] K. J. Baeg, M. Caironi, Y. Y. Noh, Advanced Materials 2013, 25, 4210; S. Bae, H. Kim, Y. Lee, X. F. Xu, J. S. Park, Y. Zheng, J. Balakrishnan, T. Lei, H. R. Kim, Y. I. Song, Y. J. Kim, K. S. Kim, B. Ozyilmaz, J. H. Ahn, B. H. Hong, S. Iijima, Nature Nanotechnology 2010, 5, 574; F. C. Krebs, J. Fyenbo, M. Jorgensen, Journal of Materials Chemistry 2010, 20, 8994; S. R. Forrest, Nature 2004, 428, 911.
[2] S. H. Ahn, L. J. Guo, Advanced Materials 2008, 20, 2044; S. Ahn, M. Ganapathisubramanian, M. Miller, J. Yang, J. Choi, F. Xu, D. J. Resnick, S. V. Sreenivasan, "Roll-to-Roll Nanopatterning Using Jet and Flash Imprint Lithography", presented at *Conference on Alternative Lithographic Technologies IV*, San Jose, CA, 2012 Feb 13-16, 2012; C. Stuart, Y. Chen, Acs Nano 2009, 3, 2062; J. John, Y. Tang, J. P. Rothstein, J. J. Watkins, K. R. Carter, Nanotechnology 2013, 24.
[3] S. H. Ahn, L. J. Guo, Acs Nano 2009, 3, 2304.
[4] Y. Deng, P. Yi, L. Peng, X. Lai, Z. Lin, Journal of Micromechanics and Microengineering 2015, 25.
[5] M. D. Fagan, B. H. Kim, D. Yao, Advances in Polymer Technology 2009, 28, 246.
[6] K. Koch, B. Bhushan, Y. C. Jung, W. Barthlott, Soft Matter 2009, 5, 1386; E. Sogaard, N. K. Andersen, K. Smistrup, S. T. Larsen, L. Sun, R. Taboryski, Langmuir 2014, 30, 12960.
[7] A. B. Christiansen, J. Clausen, N. A. Mortensen, A. Kristensen, Applied Physics Letters 2012, 101.
[8] J. Clausen, A. B. Christiansen, J. Garnaes, N. A. Mortensen, A. Kristensen, Optics Express 2012, 20, 4376; K. Kumar, H. G. Duan, R. S. Hegde, S. C. W. Koh, J. N. Wei, J. K. W. Yang, Nature Nanotechnology 2012, 7, 557; J. S. Clausen, E. Hojlund-Nielsen, A. B. Christiansen, S. Yazdi, M. Grajower, H. Taha, U. Levy, A. Kristensen, N. A. Mortensen, Nano Letters 2014, 14, 4499.
[9] H. Tan, A. Gilbertson, S. Y. Chou, Journal of Vacuum Science & Technology B 1998, 16, 3926.
[10] R. Frenkel, B. Kim, D. Yao, Machines 2014, 2, 299.
[11] C. Sollogoub, E. Felder, Y. Dernay, J. F. Agassant, P. Deparis, N. Mikler, Polymer Engineering and Science 2008, 48, 1634.
[12] T. Simone, Ø. Peter Friis, M. Marco, C. Thomas Lehrmann, C. Jiri, M. Rodolphe, T. Rafael, Journal of Micromechanics and Microengineering 2012, 22, 115008.
[13] D. G. Yao, B. Kim, Journal of Micromechanics and Microengineering 2002, 12, 604.

[14] S. Information.
[15] **H. Hertz**, J. Reine und Angewandte Mathematik 1882, 92.
[16] D. Yang, Z. Xu, C. Liu, L. Wang, Colloids and Surfaces a-Physicochemical and Engineering Aspects 2010, 367, 174.
[17] M. Matschuk, N. B. Larsen, Journal of Micromechanics and Microengineering 2013, 23.
[18] D. Y. Kwok, L. K. Cheung, C. B. Park, A. W. Neumann, Polymer Engineering and Science 1998, 38, 757.
[19] A. Gradys, P. Sajkiewicz, A. A. Minakov, S. Adamovsky, C. Schick, T. Hashimoto, K. Saijo, Materials Science and Engineering a-Structural Materials Properties Microstructure and Processing 2005, 413, 442.
[20] J. T. Xu, P. J. Ding, Z. S. Fu, Z. Q. Fan, Polymer International 2004, 53, 1314; A. J. Peacock, Journal of Macromolecular Science-Polymer Reviews 2001, C41, 285.
[21] J. E. K. Schawe, Journal of Thermal Analysis and Calorimetry 2014, 116, 1165.
[22] C. Vasile, *Handbook of polyolefins*, Marcel Dekker, Inc., New York 2002.
[23] J. Elders, H. V. Jansen, M. Elwenspoek, W. Ehrfeld, Ieee, *DEEMO: A new technology for the fabrication of microstructures*, 1995; S. Tanzi, P. F. Ostergaard, M. Matteucci, T. L. Christiansen, J. Cech, R. Marie, R. Taboryski, Journal of Micromechanics and Microengineering 2012, 22; M. Matschuk, H. Bruus, N. B. Larsen, Microelectronic Engineering 2010, 87, 1379.

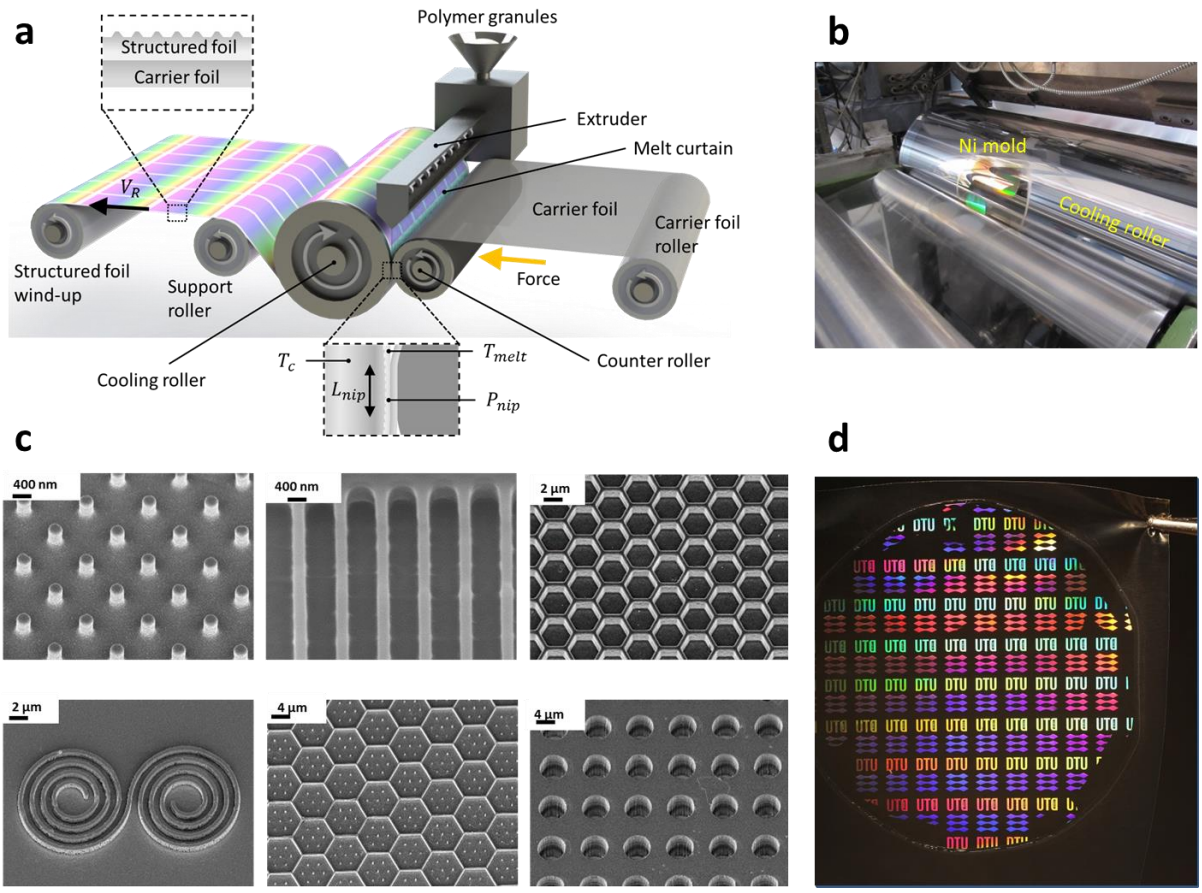

Figure 1. a: Schematic of R2R-EC process. **b:** Photograph of the cooling roller with the Ni mold mounted. **c:** Scanning electron micrographs of structures with various shapes, linewidths ranging from 400 nm to ≳1 µm, and aspect ratios ≳1 replicated in PP by R2R-EC. Images were taken at a 30° tilt angle. **d:** Example of an application of the technology; diffraction grading pattern with DTU logo produced by R2R-EC. The pattern was originated from a 100 mm Si wafer, electroformed into a Ni mold, and replicated by R2R-EC on PP foil.

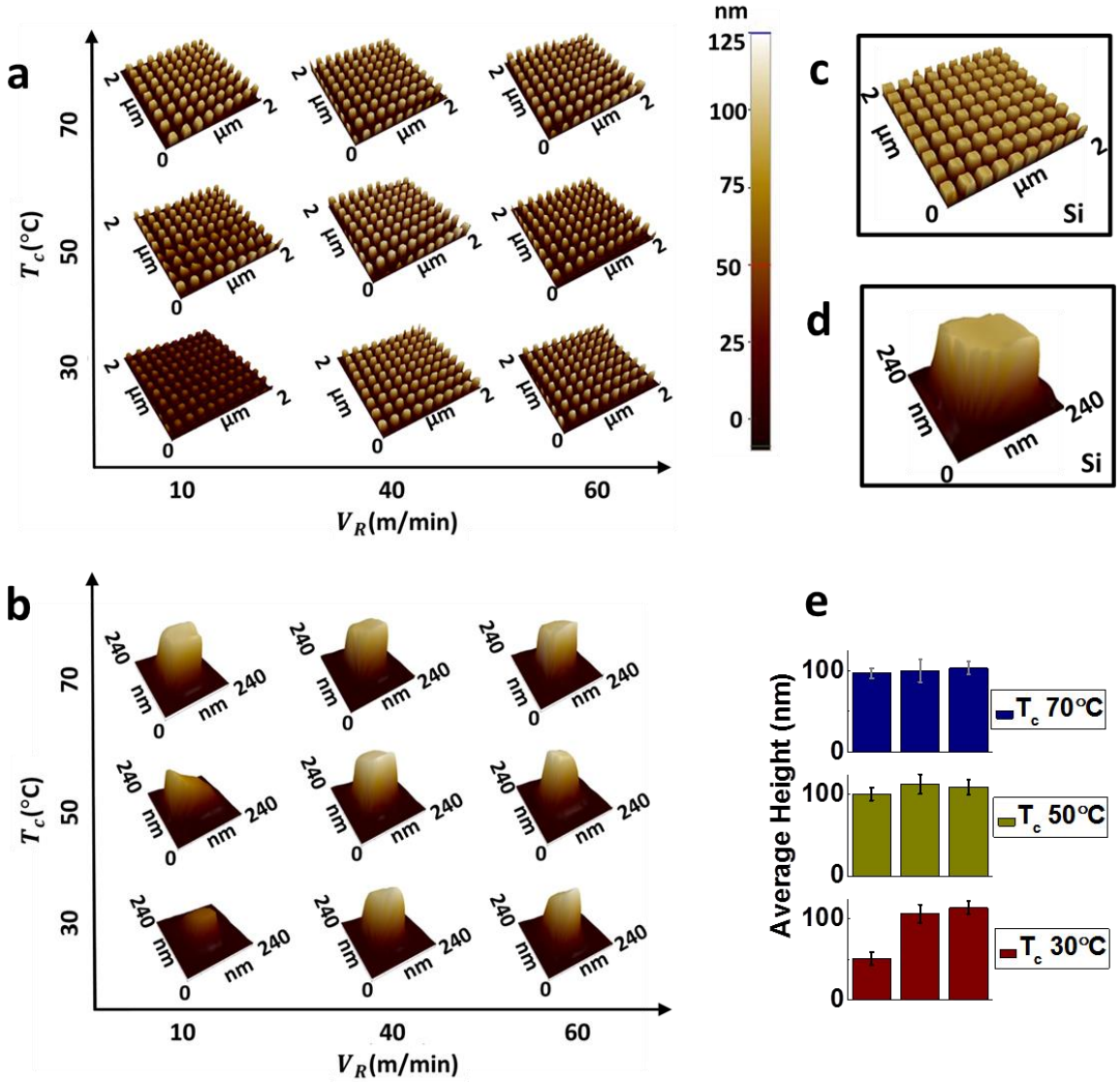

Figure 2. a: AFM images of Nano-pillar arrays replicated in PP. **b:** Single pillar extracted from arrays in (a). **c** and **d:** AFM images of the corresponding Si master structures, array (c), and single pillar (d). **e:** Average height of the pillars in (a). Error bars represent the standard deviations of heights in the 2 µm × 2 µm scan-areas.

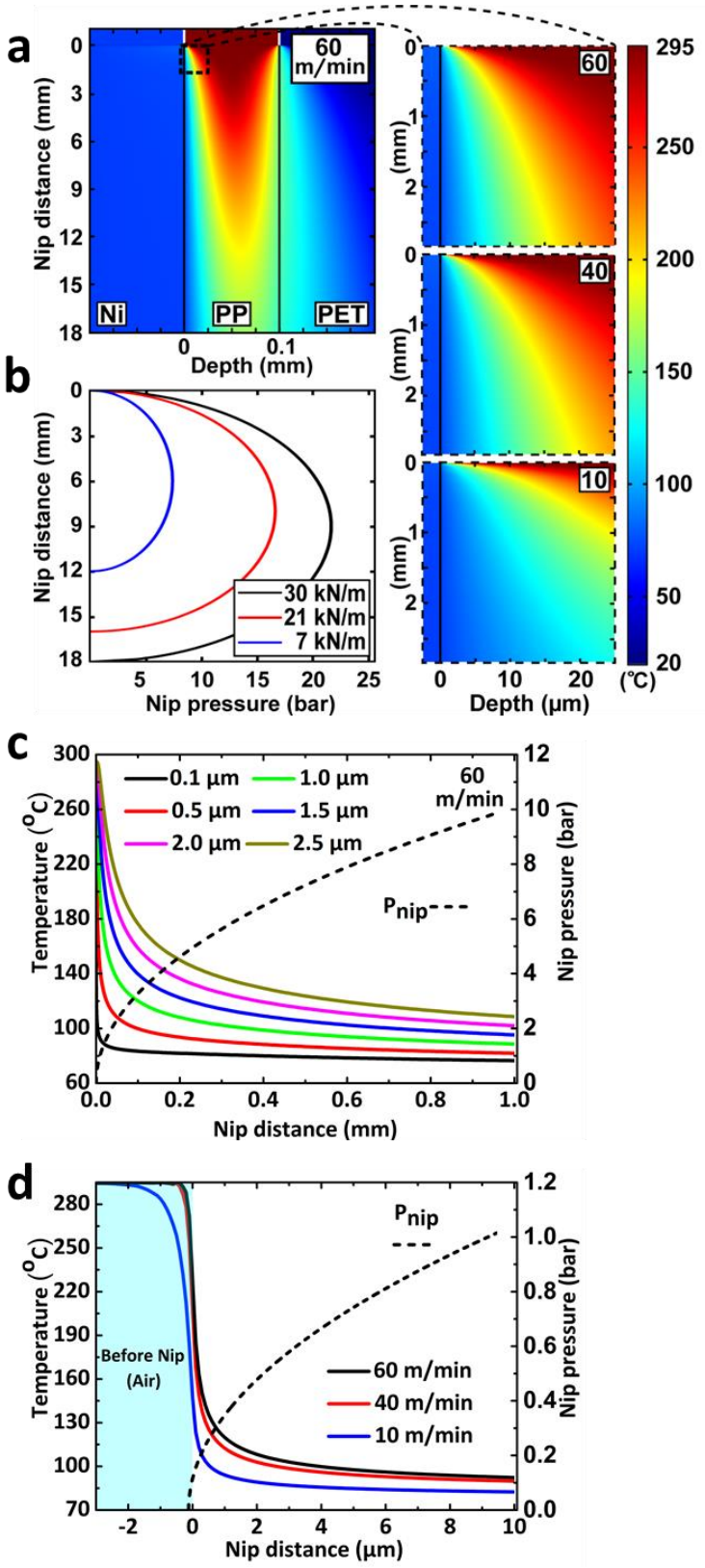

Figure 3. a: COMSOL simulation of temperature profile in the nip for $F/W = 30$ kN/m, $T_c = 70°$ C and $V_R = 60$ m/min. Right panel shows temperature profiles at nip entry for $V_R = 60$ m/min , 40 m/min, and 10 m/min respectively. **b:** Pressure profile in the nip for different values of F/W calculated using Equation 1. **c:** Temperature profile extracted at different distances from the mold surface from simulation in (a). **d:** Temperature profile extracted from simulation in (a) for different V_R at 100 nm from the mold surface.

The table of contents entry

Fabrication of micro- and nanostructures at line-speed 60 m/min by large-area roll-to-roll extrusion coating is demonstrated. Nanopillars with diameters 80 nm and heights 100 nm are replicated in polypropylene. The main limiting factor for replication on nanoscale is the retardation time for solidification of the melt. This surprisingly leads to better replication the higher line-speed is used for crystalline polymers.

Keywords: Extrusion coating, roll-to-roll, nanostructure, supercooled polymer, surface tension.

Swathi Murthy, Maria Matschuk, Qian Huang, Nikolaj K. Mandsberg, Nikolaj A. Feidenhans'l, Peter Johansen, Lars Christensen, Henrik Pranov, Guggi Kofod, Henrik C. Pedersen, Ole Hassager, Rafael Taboryski*
Fabrication of micro-nano structures by roll-to-roll extrusion coating

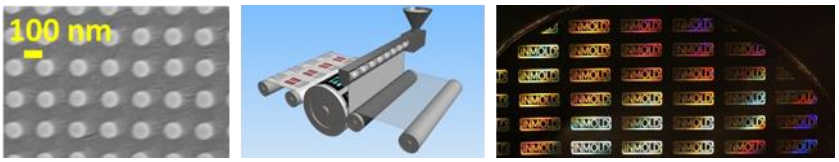

ToC figure

Copyright WILEY-VCH Verlag GmbH & Co. KGaA, 69469 Weinheim, Germany, 2013.

Supporting Information

Fabrication of micro-nano structures by roll-to-roll extrusion coating

*Swathi Murthy, Maria Matschuk, Qian Huang, Nikolaj K. Mandsberg, Nikolaj A. Feidenhans'l, Peter Johansen, Lars Christensen, Henrik Pranov, Guggi Kofod, Henrik C. Pedersen, Ole Hassager, Rafael Taboryski**

Ni mold fabrication

Polymeric nano-micro structures presented in this paper were produced by roll-to-roll extrusion coating of polymer melt against a structured nickel molds mounted on the cooling roller. The Ni molds were fabricated by electroforming from a Si master. Depending on the size of the structures, Si masters were fabricated either by deep ultra-violet lithogrphy (DUV) or electron beam (e-beam) lithography, followed by subsequent deep reactive ion etching (DRIE). For DUV lithography, various patterns with structure sizes in the range of 200 nm to few microns were spin-coated with a thin film of the photosensitive resist KRF M230Y (JSR Micro) and exposed using a DUV stepper (Canon FPA-3000 EX4). Structures smaller than 200 nm were spin coated by an e-beam resist ARN 7520 (ALLRESIST) and written by electron beam writer (JEOL-JBX9500). Subsequent to pattern exposure and development, the structures were etched into a Si wafer, by a Pegasus deep reactive-ion etching system (SPTS Technologies Ltd.), using the exposed polymer film as an etch mask. After the removal of the remaining resist film by oxygen plasma, a 20 – 100 nm thin film of nickel-vanadium alloy (7 wt% vanadium) was sputter coated (Polyteknik Cryofox Explorer 700), followed by electroplating in a galvanic nickel bath to form 175 – 200 µm thick nickel molds (Technotrans microform.200). Finally, nickel molds were coated with an FDTS antistiction layer to ease demold from the Ni surface during extrusion coating. The Ni molds originating from DUV lithogaphy were coated with a triple layer FDTS coating (Al_2O_3/SiO_2/FDTS) by the Danish Technological Institute, Taastrup, Denmark. Nickel molds made by electron beam lithography were first coated with Al_2O_3 by atomic layer deposition (Picosun ALD model R200) and subsequently with FDTS by molecular vapor deposition (Applied Microstructures Inc. MVD 100). The MVD process comprised the following: first a cycle with one injection of FDTS at 0.5 torr and one injection of water at 6 torr reacts for 15 minutes. Then the process chamber is evacuated and a new cycle starts until 4 cycles are completed. A summary of the process steps involved in the fabrication of Ni mold is presented in Figure S1.

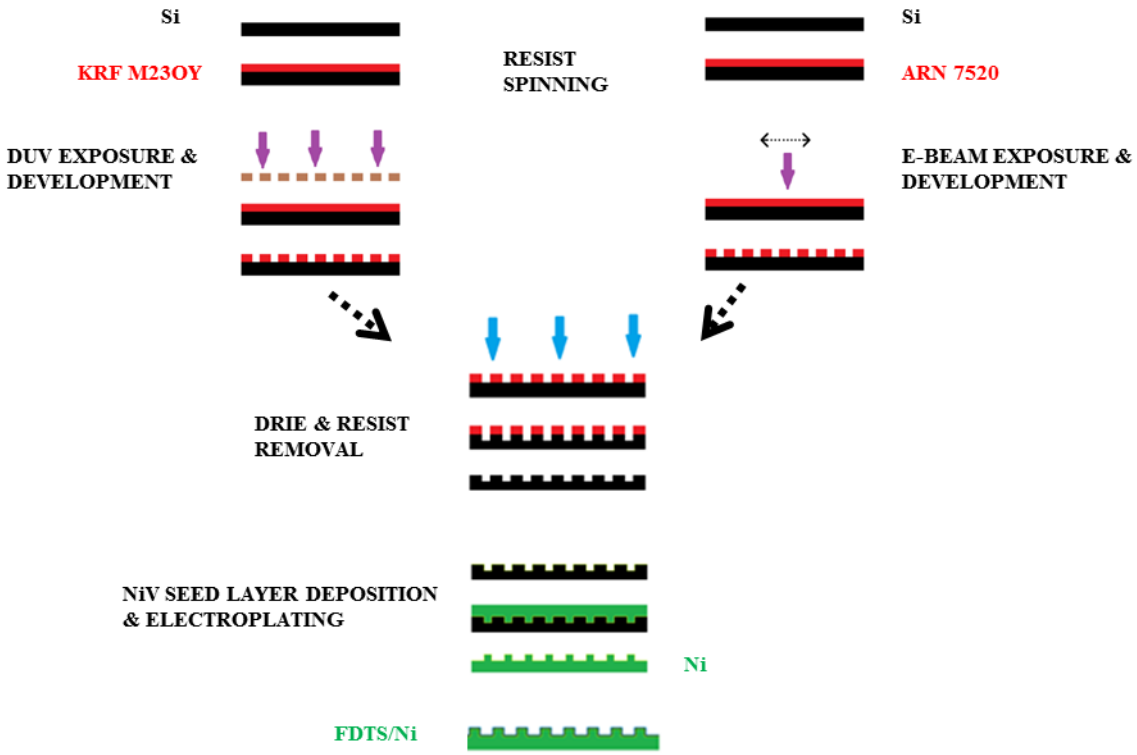

Figure S1: Schematic diagram of the nickel mold fabrication

From Si master to replication in PP

Figure S2 shows the replication of nanopillars from Si master to Ni mold and finally the nanostructured PP foil.

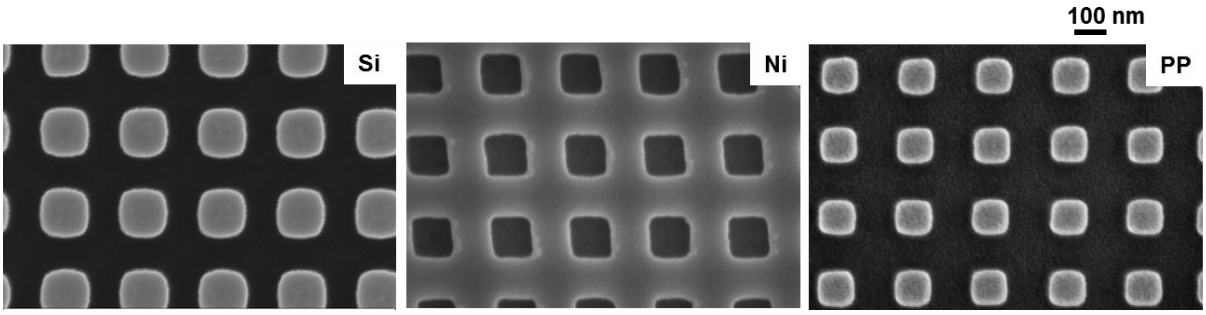

Figure S2. SEM images of nanostructures in Si master, Ni mold and PP foil fabricated by extrusion coating.

Influence of polymer material

We observed a very robust process with respect to the applicability of a wide range of process parameters yielding good replication for PP while other semi-crystalline polymers such as polyethylene (PE), polyolefin (PO), and polymethylpentene required a more tightly optimized process to replicate the very same features or did not replicate completely. For the parameter range that was used in this investigation, it was not possible to achieve a visible replication of structures in amorphous polymers such as polystyrene and cyclic olefin copolymer. In Figure

S3, the diffraction gratings have been completely replicated in PP, whereas PE shows incomplete replication and PO shows almost no replication at all for the same process conditions. In Figure S3, we see similar results, where the honey comb structures have been well replicated in PP and poorly replicated in PO.

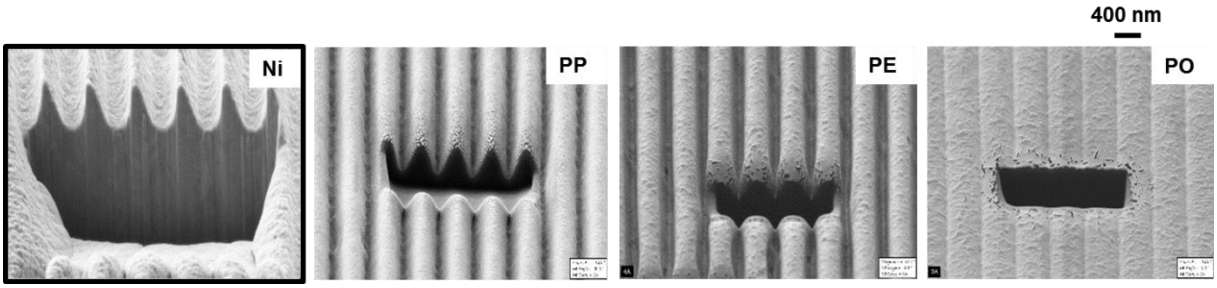

Figure S3. Focused Ion Beam-SEM images of diffraction gratings in nickel and replicas thereof, extruded in PP, PE, and PO, replicated at V_R = 20 m/min, T_c = 30° C, and F = 30 KN/m.

Influence of process parameters

Similar to injection molding and nano imprint lithography, in extrusion coating, we observed a general trend of better replication quality with higher nip force ($\boldsymbol{F}$) and higher mold temperature ($\boldsymbol{T_c}$). As shown in Figure S4, we observed complete replication of the diffraction gratings in PP at $\boldsymbol{F}$ = 30 kN/m, whereas only 60% replication at $\boldsymbol{F}$ = 7 kN/m, with other parameters kept constant.

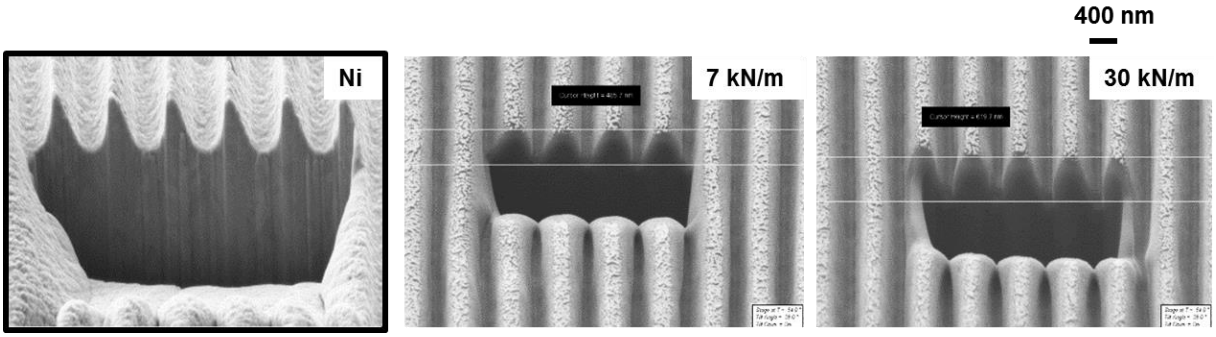

Figure S4. SEM images of samples replicated in PP produced with low nip force (F = 7 kN/m) and high nip force (F = 30 kN/m) at V_R = 20 m/min and T_c = 30° C

As shown in Figure S5, we observed complete replication of micro holes at $\boldsymbol{T_c}$ = 70° C, whereas we observed polymer flow lines, indicating incomplete replication, at lower temperatures (30° C, 50° C).

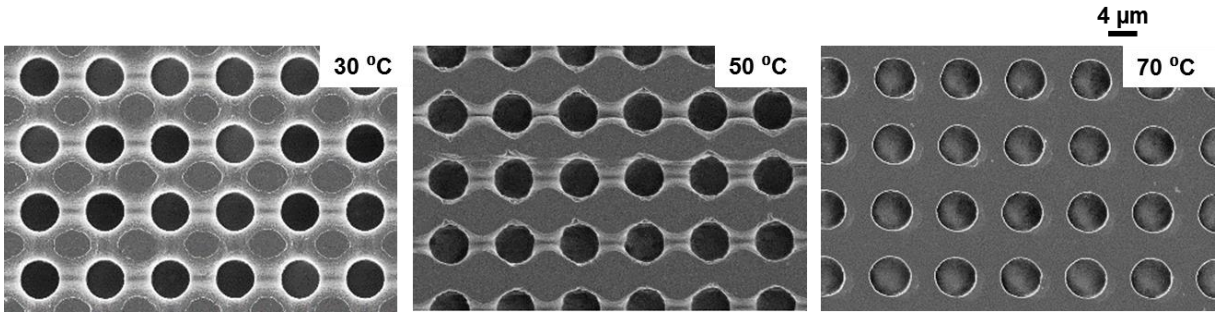

Figure S5. SEM images (top view) of microholes extruded in PP replicated with increasing roller temperature from left to right (T_c = 30°, 50°, 70° C) at V_R = 10 m/min and F = 30 kN/m. A clear improvement of the replication quality, meaning reduction in flow line formation can be observed with increasing temperature.

Influence of line-speed (V_R)

The evaluation of the sole influence of the line-speed (V_R) on the replication quality is not straight forward since the change in velocity is associated with a change in the extruded polymer film thickness. For larger structures (> 10 µm), the replication quality increased with decreasing V_R (Figure S6), for smaller microstructures (< 10µm), V_R did not seem to have dramatic influence on the replication quality (Figure S6). For nanostructures (< 200 nm), the replication improved with increasing V_R (Figure 2). For hierarchical structures (Figure S6c), the replication of nanostructures was better at higher V_R, whereas for the microstructures V_R did not seem to affect the replication quality.

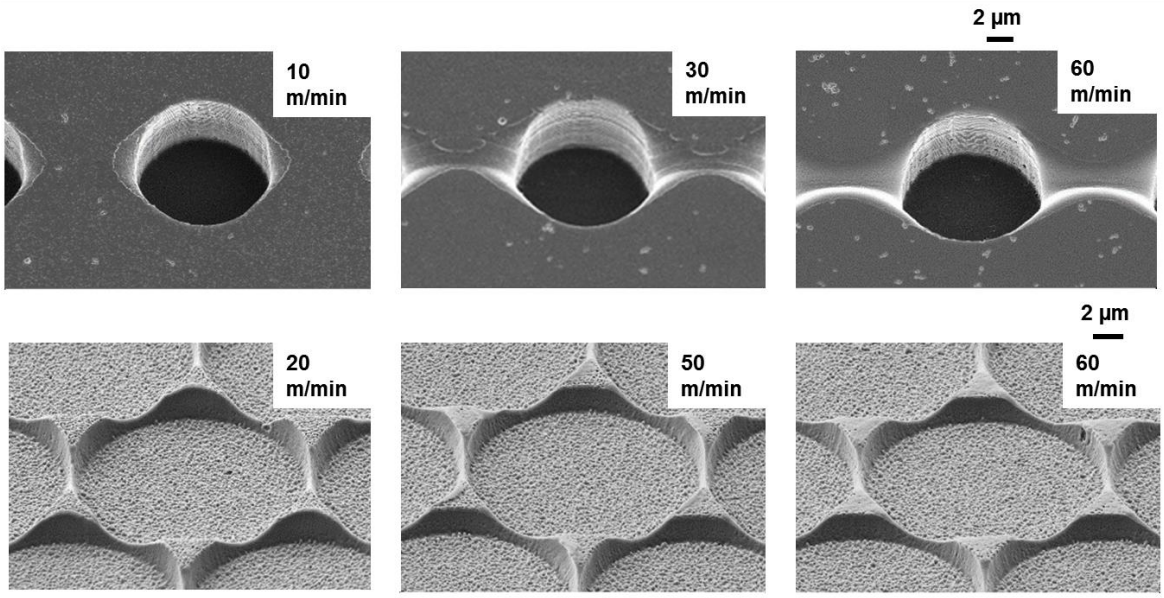

Figure S6. Top row: SEM images (30° tilt), of diameter d =11.4 µm microholes replicated in PP with increasing V_R from left to right V_R = 10, 30, 60 m/min at T_c = 30° C and F = 30 kN/m. A clear improvement of the replication quality (reduction of flow line formation) can be observed with increasing V_R. Bottom row: SEM images (30° tilt), of hexagonal microstructures of height h = 1.45 µm extruded in PP replicated with increasing V_R.from left to right V_R= 20, 50, 60 m/min at T_c = 30° C and F = 30 KN/m. The average height of the sidewalls does not change significantly, though nanostructures on top of the plateaus are worse replicated with increasing V_R.

DSC measurement of the static solidification temperature

The melting and solidification temperatures of PP-WF420HMS was determined by differential scanning calorimetry (DSC) under standard heating/cooling/heating process between -50° C and 200° C at a rate of 10° C/min. The measurements were performed using a DSC-Q1000 differential scanning calorimeter from TA Instruments. The weight of the tested sample was 6.05 mg. Nitrogen gas at a flow rate of 50 mL/min was used as the heating flow. Figure S7 shows the results of the DSC measurements. The melting temperature of PP-WF420HMS is found to be 162° C, whereas the crystallization temperature is around 123° C, which is lower than the melting temperature.

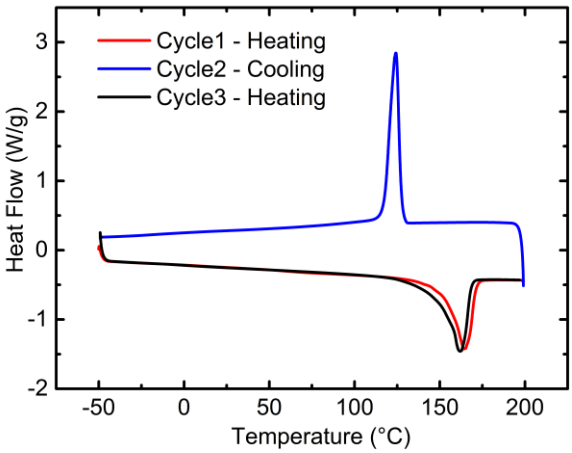

Figure S7. Results of DSC measurements for PP-WF420HMS.

Finite element modelling of the temperature distribution in the nip

The finite element modelling of the temperature in the nip was made by finite element analysis using COMSOL Multiphysics 5.0. The modelling was done using the time-independent version of the convection-diffusion equation for heat, as we were interested in the timely converged heat distribution. The heat transfer is thus solely simulated considering forced convection and diffusion. This justifies modelling the molten polymer as a solid in translation governed by Equation S1 as implemented in the standard COMSOL module 'Heat Transfer in Solids' with translational motion:

$$\rho C_p \boldsymbol{u} \cdot \nabla T = \nabla \cdot (k \nabla T). \qquad \text{(S1)}$$

Here ρ is the density, C_p is the specific heat capacity at constant pressure, $\boldsymbol{u}$ is the velocity vector, T the absolute temperature, and k the thermal conductivity. We have collapsed the problem into a 2-dimensional one since the 3rd dimension parallel to roller axle has translational symmetry in the region of interest. Equation S1 applies to each individual material domain defined in Figure S8 with appropriate values for their thermodynamic properties stated in Table S1.

Thermal Property \ Material	Ni	PP	PET
Thermal conductivity $\left(k,\ \frac{\mathrm{W}}{\mathrm{m \cdot K}}\right)$	62	0.2	0.45
Density $\left(\rho,\ \frac{\mathrm{kg}}{\mathrm{m}^3}\right)$	9000	1000	950
Heat capacity $\left(C_p,\ \frac{\mathrm{J}}{\mathrm{kg \cdot K}}\right)$	440	2300	1250

Table S1 Material properties used in the simulation.

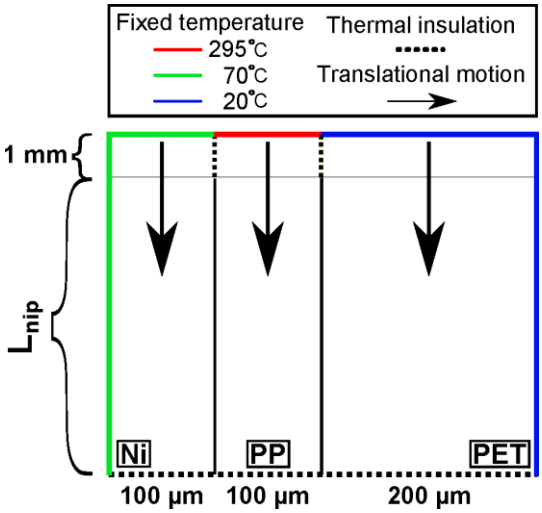

Figure S8. Schematic drawing of the simulation showing the geometry, the applied boundary conditions, and the material domains. The arrows indicate the direction of the translational motion.

The simulation has been made for 3 different line-speeds: 60 m/min, 40 m/min, and 10 m/min. Dirichlet boundary conditions were applied far away from the regions of interest. Hence, the inner part of the nickel roller was fixed at 70° C, the incoming PP melt at 295° C, and the incoming PET carrier foil at 20° C. The bottom boundary of the full simulation domain was made with thermal insulation conditions (dotted): $\boldsymbol{n} \cdot (k\nabla T) = 0$, where $\boldsymbol{n}$ is the boundary normal vector. This boundary condition was justified as the temperature of the melt had almost stabilized when exiting the nip. Insulating boundary conditions were also applied between the different materials domains at the polymer entrance to include the heat loss in the polymer melt during the stretching path in the air. This was done in order to simulate the highly insulating properties of air.

The simulation is carried out with a total number of 275.000 rectangular mesh elements with a size distribution such that regions with the largest temperature variation is attributed the smallest element size. Hence, the element size is set to change linearly, such that the smallest size is set to $\Delta x \times \Delta y = 200$ nm $\times$ 20 nm at the PP/Ni interface at the entrance of the melt in the nip region, while the largest size was set to 36 µm $\times$ 4 µm in the PET region at the exit from the nip. The x-direction is here taken along the nip length similar to the definition in Equation 1, and the y-direction is along the thickness of the foil.